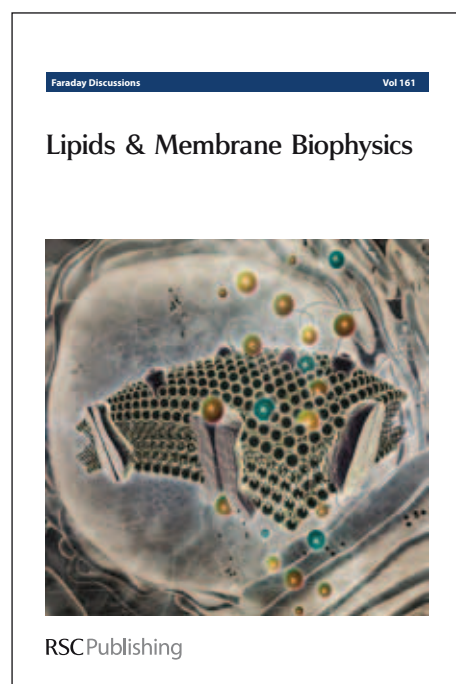# Faraday Discussions

Accepted Manuscript

This manuscript will be presented and discussed at a forthcoming Faraday Discussion meeting. All delegates can contribute to the discussion which will be included in the final volume.

Register now to attend! Full details of all upcoming meetings: **http://rsc.li/fd-upcoming-meetings**

This is an *Accepted Manuscript*, which has been through the RSC Publishing peer review process and has been accepted for publication.

Accepted Manuscripts are published online shortly after acceptance, which is prior to technical editing, formatting and proof reading. This free service from RSC Publishing allows authors to make their results available to the community, in citable form, before publication of the edited article. This *Accepted Manuscript* will be replaced by the edited and formatted *Advance Article* as soon as this is available.

To cite this manuscript please use its permanent Digital Object Identifier (DOI®), which is identical for all formats of publication.

More information about *Accepted Manuscripts* can be found in the **Information for Authors**.

The Formation of Ice Mantles on Interstellar Grains Revisited
– the effect of exothermicity –

T. Lamberts[a,b], X. de Vries,[a] and H. M. Cuppen,[a]

Modelling of grain surface chemistry generally deals with the simulation of rare events. Usually deterministic methods or statistical approaches such as the kinetic Monte Carlo technique are applied for these simulations. All assume that the surface processes are memoryless, the Markov chain assumption, and usually also that their rates are time independent. In this paper we investigate surface reactions for which these assumptions are not valid and we discuss what the effect is on the formation of water on interstellar grains. We will particularly focus on the formation of two OH radicals by the reaction $H + HO_2$. Two reaction products are formed in this exothermic reaction and the resulting momentum gained causes them to move away from each other. What makes this reaction special, is that the two products can undergo a follow-up reaction to form H_2O_2. Experimentally OH has been observed, which means that the follow-up reaction does not proceed with a 100 % efficiency, even though the two OH radicals are formed in each other's vicinity in the same reaction. This can be explained by a combined effect of directionality of the OH radical movement together with energy dissipation. Both effects are constrained by comparison with experiments and the resulting parametrised mechanism is applied to simulations of the formation of water ice under interstellar conditions.

1 Introduction

Water is one of the molecules most vital for life on Earth. How water was delivered to Earth is not completely clear. Different pathways have been suggested; including scenarios where Earth's water is of extraterrestrial origin[1]. Water frozen on interstellar dust particles could have been trapped during the accretion of dust to form our planet, or water may have been transported by comets in a later stage. In both cases, interstellar ices are at the origin of the mechanism[2,3]. In the cold regions of molecular clouds, water is formed through grain surface reactions. On the grain surface, water can be formed through simple exothermic addition reactions, where the grain serves as a third body to take up the excess energy[4].

In 2007, we performed the first microscopic astrochemical simulations on the surface formation of water in different environments: diffuse, translucent, and dense clouds[5]. This model was based on the physical and chemical information that was available at the time, which was rather poor, but it triggered many experimental studies by several different laboratories[6–9]. Because of these new experiments the surface reaction network is now much better constrained and the understanding of solid water and its precursors has improved in general. Recently, a new microscopic kinetic Monte Carlo model was developed[10] that is capable of simulating different types of water formation experiments[11,12] and that put constraints on the reaction rates of many of the reactions within the surface network. Table 2

[a] *Theoretical Chemistry, Institute for Molecules and Materials, Radboud University Nijmegen, Heyendaalseweg 135, 6525 AJ Nijmegen, The Netherlands. E-mail: hcuppen@science.ru.nl*
[b] *Raymond and Beverly Sackler Laboratory for Astrophysics, Leiden Observatory, University of Leiden, P.O. Box 9513, NL 2300 RA Leiden, The Netherlands.*

gives an overview of this network as it is currently understood[9–13]. In the present discussions, the new kinetic Monte Carlo model will be the basis for simulations under interstellar conditions. We further aim to show the importance of exothermicity of reactions and how this leads to non-Markovian behaviour and chemical desorption.

Grain surface chemistry is generally simulated by either rate equations or some stochastic method that solves the master equation. The master equation describes the change in probability to be in a certain state at a certain time. In these simulations a state is often represented by, *e.g.*, the species on the grain, their position, the temperature of the grain, etc. One of the assumptions at the root of the derivation of the master equation is that the events bringing the system from one state to the next are memoryless: the Markov chain assumption. Typical grain surface processes such as diffusion and desorption of thermalised species are effectively memoryless: they occur at much longer time scales than the (lattice) vibrations and all history about which states where previously visited is lost due to the vibrations between two transitions. For a more in-depth discussion see Ref. 14. Newly formed reaction products can behave differently however. Most grain surface reactions are highly exoergic. Part of this exothermicity will be immediately transferred to the icy mantle, but likely a substantial fraction of it remains in the reaction products making them "hot". For reactions with two or more reaction products the energy gain is distributed as momentum over the products. This will have two effects: the hot species are more likely to move and desorb than thermalised species and because they have some momentum, their movement will not be memoryless and their trajectory will therefore not follow a random walk. The energy responsible for this behaviour eventually dissipates through collisions with the grain and/or ice mantle. The extend of this effect will therefore strongly depend on the time scale for energy dissipation, which in turn depends on the local environment. Collisions with molecules making up the ice mantle are much more effective than collisions with the harder grain material which does not absorb the energy as easily.

A clear example of a reaction where non-Markovian behaviour becomes important, is the formation of two OH radicals by the reaction $H + HO_2$. This one of the few significant surface reactions in the water network that leads to two reaction products. The formed radicals will move away from each other due to their opposite relative momenta. If this reaction occurs on top of an ice or a grain surface, the species will continue to diffuse on the surface. If the reaction occurs in the bulk phase, however, they can loose their directionality through collisions with neighbouring molecules. What makes this reaction special, is that the two products can undergo a follow-up reaction to form H_2O_2. In a co-deposition experiment of O_2 and H with an overabundance of O_2 the most-likely pathway to OH formation is through this $H + HO_2$ reaction. Experimentally OH has been observed under these conditions, which means that the follow-up reaction of OH + OH does not proceed with a 100 % efficiency, even though the two OH radicals are formed close together in the same reaction.

In Ref. 10 we already suggested that one of the reasons why the kinetic Monte Carlo simulations cannot reproduce an appreciable amount of OH, without artificially changing physical parameters, is their inherent Markovian behaviour. Because of the assumption that the processes are memoryless, the OH radicals can travel in all directions, including towards the location where the OH radicals were initially formed. It is relatively straightforward to give reaction products some extra energy in kinetic Monte Carlo simulations, to alter their trajectory and not make it a random walk, is much harder. Without this change, however, newly formed OH radicals can easily meet again and react.

To constrain the time scale for energy dissipation is not straightforward. Some information is available for photoproducts of water ice photodissociation by Molecular Dynamics simulations[15–17], which are determined by Newton's equations of motion and do not assume Markovian behaviour. But these results are limited to a water-rich environment and they may not be applicable to the formation of the first monolayers of the water ice mantle.

Dulieu *et al.*[18] showed in a combined experimental and simulation study that the chemical desorption of water-related species can be much higher in the monolayer regime. Garrod *et al.*[19] already suggested the importance of chemical desorption for, *e.g.*, the gas phase detection of methanol in cold dark clouds. This work was based on the Rice-Ramsperger-Kessel (RRK) theory which relates the excess energy and the binding energy of species to a desorption probability. They modified this theory by adding an unconstrained a parameter which they chose to be 0.1. Later Cazaux *et al.*[20] studied the influence of chemical desorption on the gas phase composition by applying a KMC model, similar to one of Cuppen and Herbst[5], but specifically focusing on the impact on the gas phase and on fractionation. In the present paper, we vary the time scale for thermalisation and we will show how this affects the overall evolution of the grain mantle. We will not only focus on chemical desorption but also on its influence on the grain surface chemistry and ice structure. The parameters that corresponds best to our experiments will be applied in Section 4 to model the evolution of a grain in diffuse cloud, translucent cloud and dense cloud conditions.

2   Methodology

The formation of water is simulated by microscopic kinetic Monte Carlo simulations. For a detailed description of the method we refer to Ref. 14. The program and its parametrisation are described in detail in Refs. 5 and 10. Here, we briefly describe the main characteristics of these models. This is followed by a description of the adaptations that were implemented to overcome the use of empirically fitted parameters, replacing them by more physically relevant values. Finally we highlight the differences between experimental and astrochemical simulation runs.

The grain is represented by a lattice model in which each lattice site can be occupied by one of the species from Table 1. Each species in the lattice has 6 neighbours and 12 nearest neighbours, corresponding to a primitive cubic lattice. The total binding energy, $E_{\text{tot,bind}}$, for each species to a site is calculated by additive contributions of its neighbours. Nearest neighbours add a contribution of E and next-nearest neighbours of $E/8$. Values for E are quoted in Table 1. The neighbour below the particle adds a double contribution ($2E$). Small species, *i.e.*, H, H_2, OH, and O, are allowed to occupy interstitial sites in the ice. This is included to account for the experimentally observed penetration of H atoms into solid O_2. Diffusion of these species to subsurface positions only occurs when an O_2 or a HO_2 molecule is atop the final position, since penetration in water-like structures has not been observed experimentally. Larger species can be present in the intermediate layer, though, as a result of the positioning of reaction products.

Table 1 Species in the model and their corresponding binding energy contribution, E, in Kelvin depending on the specific environment.

	Grain	H, H_2, O	Rest
H	105	10	70
H_2	80	10	50
O_2	240	240	240
OH	210	20	210
O_2H	630	60	630
H_2O_2	1370	140	1370
H_2O	1260	130	1260
O	260	30	260
O_3	630	60	630

After the deposition of a species on the grain, it can desorb, diffuse, react or dissociate.

Each event is assumed to be thermally activated and the event rate is calculated using

$$k = \nu \exp\left(-\frac{E_{a,i}}{T}\right) \tag{1}$$

with $E_{a,i}$ the activation energy (or barrier) for process i in Kelvin and ν the attempt frequency, which is approximated by the standard value for physisorbed species, $\frac{kT}{h} = 10^{12}\,\mathrm{s}^{-1}$. Desorption can only occur if a species is positioned in the top layer and depends on the total binding energy of the site. Diffusion can occur to each of the 18 neighbouring sites, provided that this site is empty. If the site is full, the small species have a probability to move to a corresponding interstitial site. Hopping events are calculated taking into account the binding energy contribution to the site as well as a term to ensure microscopic reversibility. Reactions can occur with co-reactants occupying one of the 6 nearest-neighbour and interstitial sites. Photodissociation only occurs in the interstellar simulations under the influence of the interstellar radiation field with

$$k = \alpha_{\mathrm{photo}} \exp(-\gamma_{\mathrm{photo}} A_{\mathrm{V}}) \,, \tag{2}$$

or through cosmic-ray induced photons

$$k = \alpha_{\mathrm{cr\,photo}} \zeta \,, \tag{3}$$

where ζ is the cosmic ray ionization rate which is taken to be $1.3 \cdot 10^{-17}\,\mathrm{s}^{-1}$. Table 2 presents an overview of the chemical and photodissociation reactions included in our model. Surface reaction rates can be found in Lamberts et al.[10] and photodissociation rates in van Dishoeck et al.[21]. Deviations from these literature values are discussed in Section 2.1.

2.1 Adaptations of the Monte Carlo routine

The kinetic Monte Carlo simulation study of Lamberts et al.[10] could only reproduce the experimental observation of significant OH abundances, if the mobility of OH radicals and the barrier for OH + OH reaction were artificially increased. The values required were not consistent with other independent estimates of the OH mobility and OH + OH reaction barrier[22], but were necessary to prevent immediate recombination of the two OH radicals to form H_2O_2. Moreover, to ensure the correct ratio between formed OH and H_2O_2 a fixed branching ratio for the reaction H + HO_2 leading to 2 OH and to H_2O_2 was chosen. The latter might, however, be the result of a two step process: H + $HO_2 \rightarrow$ 2 OH $\rightarrow H_2O_2$.

In the present paper, both the diffusion and activation barrier have been adjusted to values of 210 and 0 K, respectively, and the product channel H + $HO_2 \rightarrow H_2O_2$ is removed. A physical explanation for the experimental detection of OH is the initial opposite relative momentum that two reaction products get upon reaction. To emulate this, we made two additional adaptations to the program described by Lamberts et al.[10]. The two reaction products in the first reaction will be allowed to react or move with a directional bias, such that a higher probability is given to moving in the opposite direction of the other OH radical. The total hopping rate remains the same. The directionality is retained as long as the species is excited, i.e., when the temperature of the species is higher than the temperature of the surface. Typically this allows for one to three directional hops to be performed.

Furthermore, species that are formed during an exothermic reaction resulting in two or more reaction products get a certain energy gain that can be utilized to enhance their mobility: increased hopping and desorption rates. The excess energy is expressed in terms of temperature, T_{ex} and is distributed over the produced species inversely proportional to their masses, following conservation of momentum[17], and the energy gained by species A in a reaction with products A and B is therefore $T_{\mathrm{gain,A}} = T_{\mathrm{ex}} \frac{m_B}{m_A + m_B}$. We use the following notations: T_{ex} is the excess energy of the reaction, T_{gain} is the energy given to a specific

Table 2 List of surface and photodissociation reactions used in the current model. For their corresponding rates we refer to Cuppen and Herbst[5], Lamberts *et al.*[10].

Temperature-independent reactions				
H	+	H	$\rightarrow$	H_2
H	+	O_2	$\rightarrow$	HO_2
H	+	HO_2	$\rightarrow$	products
				OH + OH
				H_2O_2
				H_2 + O_2
				H_2O + O
H	+	O	$\rightarrow$	OH
O	+	O	$\rightarrow$	O_2
H	+	O_3	$\rightarrow$	O_2 + OH
H	+	OH	$\rightarrow$	H_2O
Temperature-dependent reactions				
H	+	H_2O_2	$\rightarrow$	H_2O + OH
H_2	+	O	$\rightarrow$	OH + H
H_2	+	HO_2	$\rightarrow$	H_2O_2 + H
H_2	+	OH	$\rightarrow$	H_2O + H
OH	+	OH	$\rightarrow$	products
				H_2O_2
				H_2O + O
O	+	O_2	$\rightarrow$	O_3
Photodissociation reactions				
OH			$\rightarrow$	O + H
H_2O			$\rightarrow$	OH + H
O_2			$\rightarrow$	O + O
O_3			$\rightarrow$	O_2 + O

reaction product directly after reaction and T_{species} is the temperature of a species at any given time. For the experimental simulations, the energy is distributed (almost) equally between two products for the dominant reactions, since these products are of (nearly) equal mass. For the interstellar conditions where photodissociation reactions and the reaction $H_2 + OH \longrightarrow H_2O + H$ determine the chemistry to a large extend, T_{gain} becomes very different for the two products.

In the original simulations by Lamberts *et al.*[10] an arbitrary, small excess energy of only 100 K for each reaction product, regardless of their number, was included in the model. The event time of the next event for reaction product was then calculated using

$$\Delta t = -\frac{\ln X}{k_{\text{tot}}(T_{\text{species}})} \qquad (4)$$

with X a pseudo-random number between 0 and 1 and k_{tot} the sum of all rates (diffusion, desorption, and reaction) for this molecule. These rates were considered constant during Δt for a temperature T_{species}, that was set equal to $T_{\text{gain}} = 1/2\ T_{\text{ex}}$ after reaction. This energy was dissipated through hopping events, where each diffusion step reduces T_{species} by an arbitrary factor of 1.6. After 10^{-8} s, the local temperature of the excited species was set back to the temperature of the surface. This is based on the assumption that a molecule on the surface will be thermalised after 10 ns. The species were found to either react immediately to form a new molecule or remain in their initial configuration for times

much longer than 10 ns. The outcome of the simulation results is therefore not too sensitive to the exact choice of this time scale.

The assumption that the rates remain stationary during Δt is a rather crude approximation. To be able to study the effect of thermalisation, we have changed the algorithm which determines Δt to accommodate the effect of changing rates, *i.e.*, including energy dissipation. The dissipation of the energy is expected to be exponential[23]. To reduce the computational complexity of an exponential energy loss, a simpler expression (Eq. (5)) was suggested by Cuppen and Hornekær[24]. The sensitivity of the model to the exact functional form was checked and found to be small. The initial temperature gain is assumed to decay following

$$T'(t) = \max\left(T_{\text{surf}}, \frac{T_{\text{gain}}}{(1 + B\,(t_{\text{r}} - t_{\text{a}}))^2}\right) \qquad (5)$$

where t_{r} is the time at which the reaction occurred. A similar model was applied in Ref. 24. The parameter B can be chosen freely. Here two types of B parameters are used: B to describe the decay in the presence of an ice mantle and B_{grain} the decay on a bare grain surface. The varying temperature leads to non-stationary rates and the kinetic Monte Carlo time step cannot be determined in the usual way for this situation (see also Ref. 14). We applied the method of Jansen[25] to obtain the time step, using Eq. (5) instead of a linearly increasing temperature.

Here we assume that the total T_{ex} that is distributed over the two reaction products is never larger than the maximum exothermicity of the reactions included in the network. The main effect that we believe the excess energy has on the evolution of the ice species is by moving reactants over a large enough distance that they will not be able to react together. A large part of the energy is thought to be dissipated through (internal) rotational and vibrational modes and interaction with the substrate, but the time scales involved in this dissipation are expected to be considerably smaller than those for the translational excitation. Rotational excitation might change the reaction rates because of a change in incoming angle and, moreover, rotational and/or vibrational excitation will most likely affect the energetics involved in the reaction. However, most ice reactions are diffusion limited and we expect these effects not to dominate.

2.2 Experimental vs. Interstellar simulations

There are a few differences between the simulations of the experimental conditions and the simulations of interstellar ices. One of the differences is the composition of the gas phase (see also Section 4). The H-atom flux for experimental conditions is chosen to be 5×10^{12} atoms cm^{-2} s^{-1}, in agreement with the experimental fluxes used in Refs. 11 and 12 multiplied by a sticking fraction of 0.2. The other species arriving at the surface are H_2 and O_2, for an experimental simulation and H_2 and O under interstellar conditions. Under interstellar conditions the flux is determined by

$$f_{\text{A}} = \frac{v_{\text{A}} n(\text{A}) n_{\text{H}}}{4} \qquad (6)$$

with $n(\text{A})$ the relative gas phase abundance of species A, n_{H} the total hydrogen density, and v_{A} the mean velocity of species A in the gas. For a cloud with a temperature of 20 K and a density of $n_{\text{H}} = 10^4$ cm^{-3} and half of its in hydrogen in the form of H atoms, the H atom flux is 1.6×10^8 atoms cm^{-2} s^{-1}. The initial oxygen atom abundance is $3 \times 10^{-4}\,n_{\text{H}}$ and slowly diminishes over the course of the simulation to account for the freeze-out of the O atoms in terms of the newly formed surface species.

Besides the large difference in order of magnitude between the fluxes, there is also a change in the time scale over which the simulation is run. Experimental simulations last up to the length of the experiment (an hour), whereas astrochemical simulations are

Table 3 Summary of the parameters chosen for all experimental simulations.

#	H + HO$_2$ %	$E_{a, \text{OH diff}}$ (K)	$E_{a, \text{OH + OH react}}$ (K)	B (s^{-1})	B_{grain} (s^{-1})	T_{ex} (K)	Directionality
I[10]	56:32:2:7	105	600	–	–	100^a	off
II	91:0:2:7	210	0	–	–	100^a	off
III	91:0:2:7	210	0	10^{12}	10^{12}	200	on
IV	91:0:2:7	210	0	10^{12}	10^{12}	1000	on
V	91:0:2:7	210	0	10^{12}	10^{12}	1400	on
VI	91:0:2:7	210	0	10^{12}	10^{12}	2000	on
VII	91:0:2:7	210	0	10^{11}	10^{11}	1400	on
VIII	91:0:2:7	210	0	10^{13}	10^{13}	1400	on
IX	91:0:2:7	210	0	10^{13}	10^{13}	2000	on

^{a} A $T_{\text{gain}} = \frac{1}{2}T_{\text{ex}}$ of 100 K is given to each product, regardless of the number of products and their masses.

associated with time scales typical for dense clouds, *i.e.*, $10^5 - 10^6$ years[26]. Here we can cover between 4×10^4 and 2.5×10^5 years. Finally, the photodissociation events occur only in the interstellar simulations, where H$_2$O, H$_2$O$_2$, O$_3$, HO$_2$, and OH are allowed to photodissociate with a rate similar to their gas phase rate.
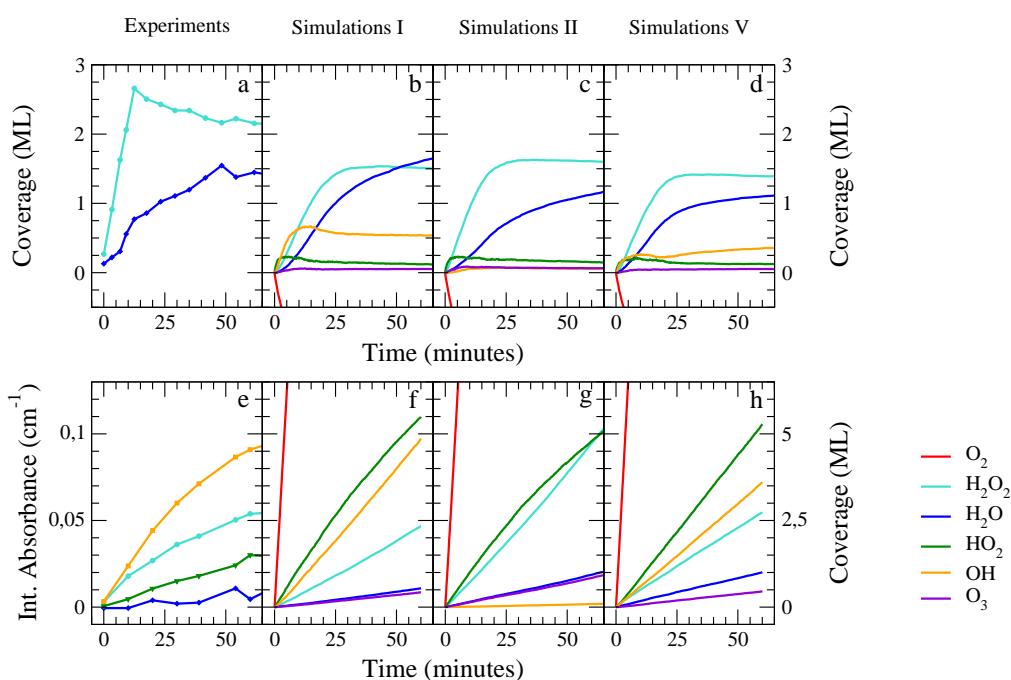
3 Simulations of experiments

Fig. 1 Evolution of the surface abundances of O$_2$, OH, HO$_2$, H$_2$O, H$_2$O$_2$ and O$_3$ as a function of time; (a) and (e) experimentally[12], (b) and (f) simulations I from Table 3, using the parameters from Ref.[10], (c) and (g) simulations II, using only physical parameters, (d) and (g) simulations V, using best fit parameters from this work (d).

Here, we present and discuss kinetic Monte Carlo simulations of the following four experiments: sequential hydrogenation of O$_2$ at 15 K and 25 K and codeposition of O$_2$ and H at 15 K and 25 K. Following the approach from Ref. 10 we have chosen to reproduce these experimental results since they are representative for different experiments of the O$_2$ + H reaction route. The experimental surface abundances are reproduced as closely as possible, but using parameters based on chemical and physical arguments rather than empirical ones
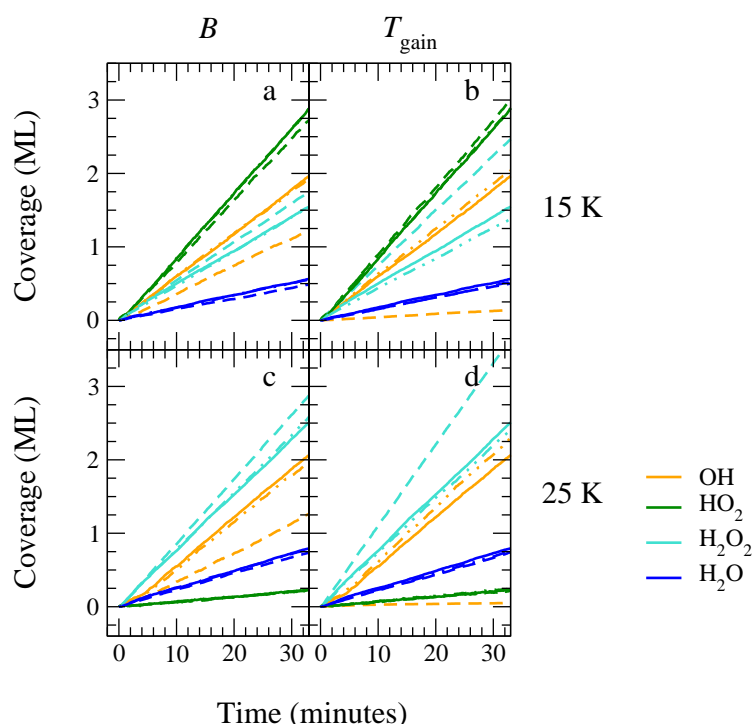
Fig. 2 Evolution of the surface abundances of OH, HO_2, H_2O, H_2O_2 and O_3 as a function of time for 15 K and 25 K with different values for B and T_{ex}. Solid lines indicate $B = 10^{12}$ s^{-1} and $T_{ex} = 1400$ K. Dashed lines indicate the lower value for B or T_{ex}, dashed-dotted lines indicate the higher value. Simulations V, VII and VIII are depicted in panels (a) and (c), runs III, V and VI in panels (b) and (d).

which was done in the previous study. As mentioned above, one of the crucial parameters was found to be the OH mobility rate combined with the OH+OH reaction barrier. These, as well as different choices for T_{ex} and B and B_{grain} (Eq. 5) are changed in the current study to obtain a set of, physico-chemically acceptable, best fit parameters that can be implemented in simulations run over astrochemically relevant time scales. The parameters chosen for all simulations are summarized in Table 3. The experimental simulations were performed on a more smooth surface, analogous to the polished gold substrate used in the experimental set-up. Since the experimental studies are all bulk studies, the exact nature of the initial substrate is only of marginal influence.

Figure 1 shows a comparison of the time evolution of surface abundances that are experimentally obtained[12] with simulated results for runs I, II and V. Changing the set of parameters from simulation I to II encompasses the use of more realistic values. For instance, the barrier for the OH + OH reaction is removed following the recommended gas phase value from Atkinson *et al.*[22]. The new value, however, results in a poorer agreement with the experimental results for the co-deposition simulations. In general, this is due to the fact that all OH radicals produced by the reaction H + HO_2 are used in a follow-up reaction to subsequently produce H_2O_2 since there is no preventing mechanism. This is clear from the decrease of the OH surface abundance by 5 ML and the simultaneous increase of the H_2O_2 abundance by 2.5 ML. For the sequential hydrogenation at 15 K, a similar effect is observed and all H_2O is subsequently formed through the reactions H + $H_2O_2 \rightarrow H_2O$ + OH and H + OH $\rightarrow H_2O$. H_2O is slightly underproduced since there are not enough OH radicals available for reaction, but no large discrepancies with respect to the experiment are observed.

To improve the reproduction of the experimental co-deposition surface abundances, directional hopping is included as well as the use of non-stationary excess energy. In Figure 2 co-deposition simulations III and V-VIII are presented for 15 K and 25 K.

Table 4 Summary of the effect of the B and T_{ex} parameters on the formation of OH and subsequent behaviour in the experimental simulations.

#	T_{ex} (K)	B (s^{-1})	T_{surf} (K)	$\frac{2OH \rightarrow products}{HO_2 + H \rightarrow 2OH}$	$\frac{[2OH]}{[H_2O_2]}$	Diffusion ('hot' events/sp)
III	200	10^{12}	15	0.90	0.03	1.0
IV	1000	10^{12}	15	0.62	0.49	1.1
V	1400	10^{12}	15	0.55	0.66	1.4
VI	2000	10^{12}	15	0.50	0.75	2.2
VII	1400	10^{11}	15	0.62	0.35	4.4
VIII	1400	10^{13}	15	0.55	0.66	1.1
IX	2000	10^{13}	15	0.50	0.79	1.1
III	200	10^{12}	25	0.90	0.01	1.0
IV	1000	10^{12}	25	0.69	0.32	1.2
V	1400	10^{12}	25	0.63	0.42	1.4
VI	2000	10^{12}	25	0.60	0.49	2.2
VII	1400	10^{11}	25	0.72	0.22	4.8
VIII	1400	10^{13}	25	0.64	0.40	1.1
IX	2000	10^{13}	25	0.62	0.42	1.1

Firstly, the dependence of the surface abundances on T_{ex} is manifested mainly through a difference in the OH versus H_2O_2 production. A higher mobility of the reaction products from the reaction $H + HO_2$ allows them to move away from each other and prevent subsequent reaction to H_2O_2. This can also be seen in Table 4 where the ratio of follow-up reactions over the initial $H + HO_2 \longrightarrow 2OH$ reaction is given. This ratio decreases with T_{ex}. The overall $\frac{[2OH]}{[H_2O_2]}$ abundance ratio is also affected by other reactions and desorption and can therefore not be directly derived from the first ratio. It is, however, more easily comparable to experimentally measurable quantities. Cuppen *et al.*[12] determined this ratio to be 1.6 ± 0.2 for 15 K and less than 0.5 for 25 K. The assumption was made that the bandstrength of the OH stretch mode of H_2O_2 is twice the bandstrength of that of the OH radical. If this assumption is indeed valid, a T_{ex} of 200 K is obviously not enough to allow for sufficient build-up of OH in the ice. A value of 1400 K or 2000 K appears to describe this experimental observable best.

Panels (a) and (c) in Figure 2 give the results of runs V, VII, and VIII and show the influence on B. Similar trends are observed when simulations VI and IX are compared. Again the results are also summarized in Table 4. The $\frac{2OH \rightarrow products}{HO_2 + H \rightarrow 2OH}$ ratio remains more or less unaffected with varying B, as expected since this is almost purely determined immediately after the formation of the two OH radicals. The influence of the B parameter becomes most apparent if one considers the number of diffusion events during thermalisation of a single species which is presented in the last column of Table 4. These diffusion events can bring the OH radicals to nearest-neighbour sites over a distance of approximately 3 Å, using a site density of 10^{15} sites cm^{-2}, or to next-nearest-neighbour sites over a distance of 4.5 Å. The number of diffusion events increases with decreasing B for the same T_{ex} since B controls how fast thermalisation occurs. The initial momentum of the particle is, however, determined by T_{ex} and the number of diffusion events is therefore a function of both. The average diffusion of a single species with an initial T_{ex} value of 1400 K ranges between 1.1 and 4.4 hops. Since we use a directionality for the mobility, OH will have more or less travelled in a straight line, in the opposite direction of the other OH radical formed. The OH radicals have therefore covered a spatial range of 3.3 to 20 Å. Molecular Dynamics simulations by Andersson *et al.*[15] and Arasa *et al.*[17] show that the distance travelled by an excited OH radical inside bulk, non-porous ice is approximately 2 Å. The distance travelled on top of a surface can range up to 80 Å. In our simulations, species are always restricted by either bulk molecules or neighbours residing on step edges and islands. Therefore we expect the

distance travelled by a hot reaction product to be larger than 2 Å, but considerably smaller than 80 Å. We expect a value of 10^{12} s^{-1} for the B parameter therefore to be most realistic.

Experimentally, a large drop in the HO$_2$ and OH surface abundances accompanied by a strong increase in H$_2$O$_2$ is observed upon increasing the temperature from 15 to 25 K. The decreasing OH abundance is only reproduced by simulations III; the decrease in HO$_2$ and increase in H$_2$O$_2$ are seen in all simulations. Experimentally, at 15 K OH is more abundant, whereas at 25 K H$_2$O$_2$ is more abundant. Taking this into account leads to best fit parameters of $B = 10^{12}$ in combination with T_{ex} = 1400 or 2000 K. In conclusion, our simulations of the codeposition experiments show that thermalisation is indeed an important effect which can help explain the observed behaviour.

Simulations of sequential hydrogenation experiments show, however, that the produced H$_2$O/H$_2$O$_2$ ratio for the low T_{ex} value reflect the experimental results better. Moreover, the slight decrease of the H$_2$O$_2$ abundance around 10-20 minutes od experiment is best reproduced by an excess energy of 1400 K. For this reason, we will continue to use the parameters of simulations V throughout the remainder of the paper, but we will comment in the text how the other parameter choice affects the obtained experimental simulation results.

Finally, as mentioned in the introduction, Dulieu et al. [18] studied the importance of chemical desorption of reaction products through sequential O$_2$ hydrogenation experiments where the amount of deposited O$_2$ remained in the (sub)monolayer regime. Their underlying substrate was an amorphous silicate or a graphite surface. They find substantial desorption of the formed H$_2$O molecules. This is caused, at least in part, by the lack of binding with surrounding molecules. Their (sub)monolayer system is fundamentally different from our bulk studies. Using our optimised model we indeed find a similar trend, albeit only concerning desorption of formed OH radicals. Desorption of OH radicals for a surface covered with $\sim$ 0.5 ML O$_2$ is a factor of 2.5–5 larger than on a surface covered with $\sim$ 3.5 ML O$_2$ for T_{ex} values of 1400 and 2000 K. Desorption of H$_2$O is not prominent, as expected, since a water molecule atop a water surface with one H$_2$O neighbour has a total binding energy of 5020 K in our simulations, comparable to the value reported by Dulieu et al. [18].

4   Simulations of interstellar conditions

We have chosen to run simulations under interstellar conditions, using a T_{ex} of 1400 K and $B_{ice} = 10^{12}$ s^{-1} and $B_{grain} = 10^{11}$ or 10^{12} s^{-1}. The physical conditions and relative fluxes of the different species are given in Table 5 along with the values used in the laboratory. The physical conditions are chosen equal to those in Cuppen and Herbst [5] for A2, D2, E2 and F2, representing a diffuse, translucent and two dense clouds, respectively. Also the same initial grain surface was used as in this previous study. This initial grain surface possesses a high degree of surface roughness and is therefore thought to be representative for the irregularly formed interstellar grains. For dense cloud condition II, H-atom diffusion is rapid and H-atom desorption is slow. Simulations can therefore not be run for astrophysically relevant timescales. We can however comment on the relative contribution of the H$_2$O production channels, since we find that these do not change beyond the production of one monolayer. Figure 3 shows the surface abundances for all species for two simulation runs of a typical diffuse cloud, Figure 4 for the translucent and dense cloud I conditions. Figure 5 gives cross sections of the resulting three simulated grains. Tables 6 and 7 summarize the contributions of the different reaction routes to OH and H$_2$O formation, respectively, for all four conditions.

4.1   Diffuse clouds

The simulations of the diffuse cloud conditions reach within 2×10^4 years an almost steady state situation of a more or less empty grain with a H$_2$O surface abundance of 1×10^{-3} ML
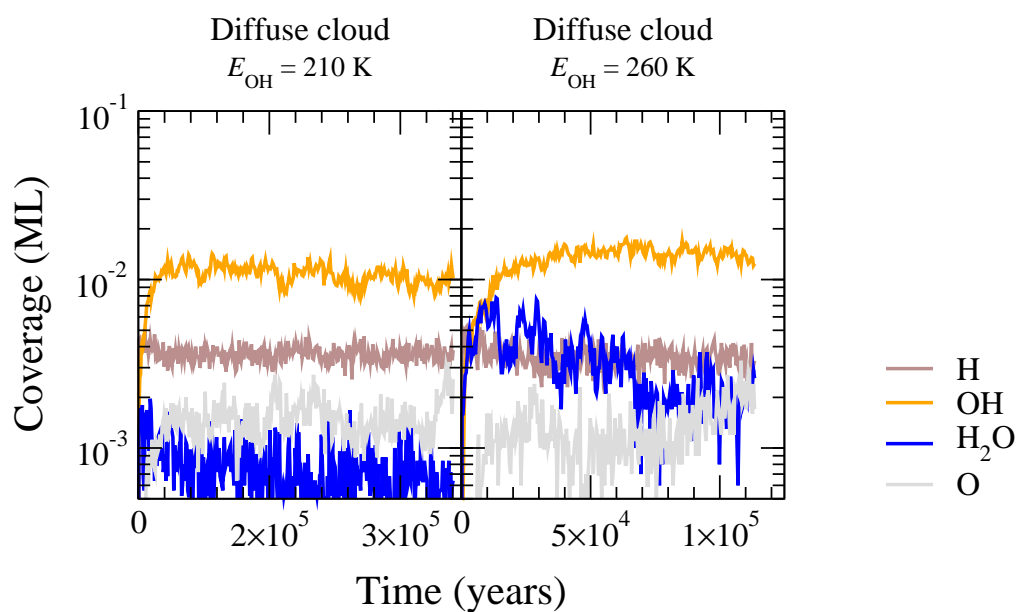
Fig. 3 Simulated surface abundances of ice species in monolayers as a function of time under two diffuse cloud conditions. Panel (a) shows the abundances for a standard run with $E_{OH} = 210$ K, panel (b) for a run with $E_{OH} = 260$ K.
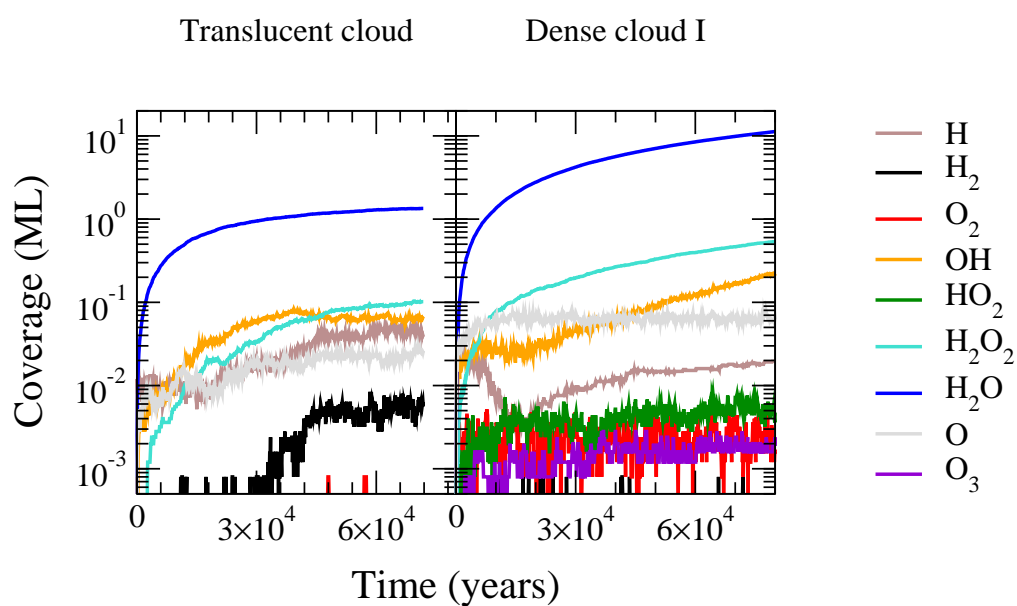
Fig. 4 Simulated surface abundances of ice species in monolayers as a function of time under (a) translucent and (b) dense cloud I conditions.

Fig. 5 Cross sections of simulated grains for the three cloud conditions: diffuse, translucent, and dense I, respectively. The grain sites are represented by black, orange is H_2, dark blue H_2O, light blue H_2O_2, yellow OH, and grey O.

Table 5 Physical conditions and initial fluxes of the reactants in the simulations under laboratory and interstellar conditions.

Parameter	Lab	Diffuse	Translucent	Dense I	Dense II
A_V (mag)	–	0.5	3	5	10
n_H (cm^{-3})	–	1×10^2	1×10^3	5×10^3	2×10^4
T_{gas} (K)	300	80	40	20	10
T_{grain} (K)	15	18	14	12	10
f_A (# cm^{-2} s^{-1})					
H	2.5×10^{13}	3.2×10^6	2.3×10^5	3.2×10^4	2.3×10^4
H$_2$	2.5×10^{13}	–	8.0×10^6	2.9×10^7	8.0×10^7
O	–	2.4×10^2	1.7×10^3	6.1×10^3	1.7×10^4
O$_2$	2.5×10^{13}	–	–	–	–

Table 6 Contributions of the different surface reaction routes to OH formation.

	T_{ex} (K)	H + HO$_2$	H + O	H + O$_3$	H + H$_2$O$_2$
Diffuse	1400	0.0	100.0	0.0	0.0
	2000	0.0	100.0	0.0	0.0
Translucent	1400	0.5	89.7	0.0	9.8
	2000	0.7	92.2	0.0	7.1
Dense I	1400	13.2	82.7	0.9	3.2
Dense II	1400	31.6	55.1	6.6	6.6

and a OH surface abundance of 0.01 ML. Deposited oxygen atoms are efficiently converted into H$_2$O through reactions with H atoms. Due to the strong radiation field for these conditions all formed water molecules are photodissociated into OH which desorbs in 48 % of the photodissociation events during steady state. The remaining OH either reacts again with H atoms to H$_2$O or is further dissociated to O and H. This cycle results in this low surface coverage of H$_2$O and OH; the total ice coverage is lower than the equivalent simulations in Cuppen and Herbst[5] (0.05 ML) and in the previous simulations H$_2$O was the dominant species. The reason for this discrepancy is the high OH photodesorption rate. We will come back to this issue later. The species that stay on the surface, fill the vacancies of the grain surface or reside near the step edges as can be seen in the left panel of Fig. 5, which shows cross sections of the simulated grain surfaces. The photodesorption rate of OH radicals on top of a grain fluctuates as function of time and appears to depend on the time-dependent, local configuration of the grain. If the water molecules are mostly present in a local configuration where the photodesorption rate is lower, their oxygen atoms will repeatedly undergo the formation-dissipation cycle resulting in lower average desorption rate. Once these atoms have desorbed the time-dependent photodesorption rate increases again until such a favourable configuration is again obtained. However, considering all dust grains in a typical diffuse cloud, these fluctuations will average out.

The photodesorption efficiency (amount of hot desorbed OH radicals devided by the number of H$_2$O photodissociation events) fluctuates between 28 and 80 % with a median value of 48 %. This is significantly higher than the values obtained by Andersson *et al.*[15]: 9 and 2 % for OH desorption *in* the first monolayer of crystalline and amorphous ice, respectively. In their case, the efficiency also depends on the local configuration. One would expect the desorption rate on top of a grain to be higher than from bulk ice because excess energy is probably easier to transfer to an molecular environment than to a more brittle grain surface. For this reason we ran additional simulations with a B_{grain} parameter of 10^{11} s^{-1}. This B_{grain} parameter is used for energy dissipation of species that do not have any molecule in their immediate vicinity. For these simulations the photodesorption efficiency of OH upon H$_2$O photodissociation behaves very similar (51 %). The steady state coverages of OH and H$_2$O remain the same for this case as can be seen in Fig. 3. Our values may

Table 7 Contributions of the different reaction routes to H_2O formation.

	T_{ex} (K)	H + OH	H_2 + OH	H + H_2O_2	OH + OH	H + HO_2
Diffuse	1400	99.5	0.0	0.0	0.5	0.0
	2000	99.8	0.0	0.1	0.1	0.0
Translucent	1400	85.4	2.4	10.4	1.8	0.0
	2000	87.6	2.2	8.7	1.5	0.0
Dense I	1400	76.7	17.6	4.0	1.0	0.7
Dense II	1400	22.5	61.6	11.3	2.4	2.2

be much higher, but concern an almost empty grain surface. The binding energy of an OH radical on top of a surface is most likely lower than of an OH embedded in a water layer. We ran some additional simulations in which we increased the binding energy of OH to the surface from $E = 210$ K to $E = 260$ K. In this case the photodesorption efficiency of OH ranges between 5 and 17 % with an average efficiency of 9 %, which is comparable to the results of Andersson *et al.* [15]. The steady state surface abundance is now 6×10^{-3} ML for H_2O and 0.02 ML for OH. Using this increased binding energy, the experimental simulations remain very similar and still reproduce the experimental observations. Finally, another parameter that is of influence on the photodesorption efficiency is T_{ex}, increasing its value to 2000 K also increases the photodesorption. In the following, all discussed simulations are parametrised according to T_{ex} of 1400 K and $B_{ice} = 10^{12}$ s^{-1} and $B_{grain} = 10^{11}$ s^{-1} and using the standard OH binding energy.

During the simulations, not only H_2O is formed, but H_2 as well. We see here that because of our rough surface, the residence time of the hydrogen atoms is not the rate limiting step, but rather the sticking probability of the hydrogen atoms to the surface. Since under these conditions the gas phase has a relatively high temperature of 80 K, the sticking probability of H atoms to the surface is relatively low (~ 33 %), but more than 47 % of all H atoms remaining on the surface react to form H_2, leading to an H_2 formation efficiency of 15 %. This is in good agreement with the results from Chang *et al.* [27], who found a recombination efficiency of ~ 10 % for temperatures as high as 21.8 K, which is enough to account for significant H_2 production in diffuse interstellar clouds. Again we can observe a time-dependent H_2 formation rate in the beginning of the simulation when the ice develops. This is because of similar arguments as for the time-dependent OH photodesorption rate. Lower E for H binding to the bare grain than 105 K results in lower H_2 formation rates, mainly because of the reduced sticking. Since we know observationally that H_2 has to be formed under these conditions, we have chosen to use this value for E. Lower values of E result in a similar production of H_2O and all other species, except H_2.

4.2 Translucent clouds

In general we observe a similar behaviour compared to the results from Cuppen and Herbst [5], *i.e.*, the competition between photodissociation and surface reaction is key. The new photodissociation rates, following van Dishoeck *et al.* [21], are higher than those previously used, but attenuate faster with visual extinction which results in lower rates at $A_V = 3$ mag.

In our present simulations the growing ice layer reaches a thickness of slightly more than a monolayer after 7×10^4 years, where a steady state seems to have been reached. Cuppen and Herbst [5] obtained surface coverages of a few monolayers under equivalent circumstances. They found that the bottom layers are heavily processed and contain more oxygen-rich species like OH, O_2, and O_3 , since these layers lose part of their hydrogen due to the photoprocessing. Here, we stay around the monolayer regime and we therefore do not see the same effect. One of the reasons for this is the higher photodesorption rate. The ice structure found in the previous work was very porous due to the heavy processing. Figure 5b a cross section of the ice surface is depicted, where only some small pores can be

found. The lack of strong porosity upon processing is in agreement with experimental work on ion irradation of water ices by Palumbo [28] and is probably caused by the exothermicity of the photoproducts that allows for restructuring.

The contribution of the various reaction routes (Tables 6 and 7) shows that most of the OH is formed through the reaction $O + H$, although the dissociation of H_2O also plays a role (see below). Even though the amount of H_2 is high, the $H_2 + OH$ route is less efficient in the formation of water ice, since the reaction is not barrierless. We observe H_2O_2 as a result of the reaction route $OH + OH$. The follow-up reaction $H + H_2O_2$ is consequently also more important for both OH and H_2O formation, more than in the previous 2007 work. The H_2O production rate decreases for increasing times. We also observe that the contributions of the various reaction routes change with time, before the steady state is reached OH is formed only through $H + O$ and H_2O only through $H + OH$. At later times, however, the contribution of $H + H_2O_2$ becomes stronger. Both the evaporation and dissociation rate of the various species also increase up to the point where the total surface coverage is ~ 0.6 ML, then the rates stabilize.

To distinguish between desorption originating from photodissociation events and from reaction heat is not trivial, hence we will only comment on it qualitatively. The largest part of the desorbing OH radicals originates from photodissociation of water. Changing the exothermicity to 2000 K leads to a larger amount of chemical desorption events, whereas increasing the binding energy of OH to the surface decreases this amount. Even though the relative contributions of the various reaction routes do not change upon changing these parameters, the final amount of (water) ice produced does. An increased desorption, regardless of the origin, decreases the ice thickness since less radicals are available for reaction.

4.3 Dense clouds

The right panel of Fig. 4 shows the surface abundance of a water covered grain for dense cloud condition I. For both dense cloud conditions I and II water ice is efficiently formed, more efficiently than in the Cuppen and Herbst [5] simulations. The main reasons for this are that H_2 does not stick to the surface as easily, which prevented many surface reactions in the earlier work, and that the ice is more compact because of the use of excess energy. The latter can be seen in the right panel of Fig. 5, where a very compact ice is formed; much more compact than in Cuppen and Herbst [5] where towers of H_2O were formed, typical for ballistic deposition [29]. In the present simulations, the formed species have some momentum to move around and find a more favourable binding site, which leads to a smoothing of the formed ice. Oba et al. [30] indeed find that ice that is formed on a surface shows more characteristics of a compact ice than ice that is deposited at similar low surface temperatures.

Under dense cloud conditions, the O_2 route becomes increasingly important, since the O/H flux ratio increases going from diffuse, to translucent to dense I and finally dense II. This can be seen in Table 6. The contribution of the $H + HO_2$ reaction to the formation of the hydroxyl radical increases. The intermediate HO_2 is formed from $H + O_2$. At the same time, we see the related reaction $O_3 + H$ increases as well. A clear difference with the Cuppen and Herbst [5] simulations is that now the O_2 channel does not exclusively proceed with H_2O_2 as an intermediate for H_2O formation. Table 7 shows that its contribution increases with density (O/H flux ratio), but not to the same extend as in the previous simulations. In the present work, most of the OH formed through the O_2 formation channel is transformed into water through the follow-up reactions $OH + H$ and $OH + H_2$. Since the first has no barrier, this reaction is preferred under most circumstances. However, under dense cloud II conditions water ice is predominantly formed through the latter reaction, since the H_2 flux becomes much higher than the H flux and the surface residence time of H_2 increases at the same time because of the low surface temperature. Indeed, the main differences between the two dense cloud conditions are the density and the grain temperature. The percentage

of intermediate species is higher for dense cloud II than for dense cloud I. This is probably because H atoms cannot convert these intermediate species into stable species as easily under these conditions. A lower temperature namely results in less H diffusion and the H-atom flux relative to the H_2 flux and O-atom flux is lower than for dense cloud I.

Photodesorption is not important here due to the high visual extinctions involved. Part of the formed water ice is returned into the gas phase, however, by chemical desorption. The 1400 K excess energy can be used for desorption when two reaction products are formed and therefore we see that chemical desorption is more efficient for the dense cloud II simulations since the contribution of reactions with two products (H_2 + OH and H + H_2O_2) is larger here. Roughly, desorption of OH is 10 and 29 % respectively, for H_2O it amounts to 5 and 13 %.

In our current model, it is not possible for intermediate species HO_2 and H_2O_2 to desorb, although these species have been observed in the gas phase[31–33]. Desorption mechanisms, other than chemical desorption, could be responsible for these observations. These mechanisms include photodesorption through cosmic ray photons or cosmic ray desorption, where a cosmic ray hit of a grain results in the desorption of most of the mantle material[34,35]. This stochastic rare event is rather hard to simulate considering a single grain, but integrated over a large cloud with many dust grains the effect can be significant. Another possible desorption mechanism that is not included here is the so-called kick-out mechanism, where a cold species desorbs as a result of a hit by a hot species. This was observed in Molecular Dynamics simulations to be important[15–17]. Experimentally this mechanism was confirmed by time-of-flight measurements of the desorption fragments of water ice photodissociation[36]. Similar conclusions were drawn for the photodesorption of N_2 in the presence of CO, where the excited CO kicks out N_2 which has no absorbance in applied photon range[37].

4.4 Comparison to observations and other models

Much of the work done since Cuppen and Herbst[5] has focussed their attention on the importance of the molecular oxygen route for water formation. Here we found that this route has the largest implications in dense clouds, as expected. A particularly interesting region to study the influence of O_2 in dense clouds is ρ Oph A, where O_2, HO_2 and H_2O_2 have been detected in recent years[31–33,38,39]. The derived abundances with respect to hydrogen are 5×10^{-8}, 1×10^{-10} and 1×10^{-10}, respectively. The hybrid moment equation approach was applied by Du and Parise[33] to model the production of interstellar H_2O_2 on the surface of dust grains. They ran a model for a range of different physical conditions and found reasonable agreement with observations for a time of 6×10^5 years, with abundance ratios of the three species of 60:3:1 in the gas phase for O_2:HO_2:H_2O_2. They use the chemical desorption mechanism introduced by Garrod et al.[19] and see that the exact setting of the a parameter has a large influence on the gas phase composition. Furthermore, the reaction OH + OH is excluded from their network and the reaction H + H_2O_2 has a lower barrier than adopted here. Both factors could increase their H_2O_2 abundance.

In our model we do not calculate any gas phase abundances, but as outlined by Öberg et al.[40] the gas phase abundance seems to reflect the composition of the co-existing ice mantles (see also Fig. 1 in Du and Parise[33]). The dense cloud simulation runs do indeed produce O_2, HO_2, H_2O_2 next to H_2O where we do not see that the O_2 abundance is much higher than for HO_2 and H_2O_2, which is likely caused by the much lower desities considered. The physical parameters determined for ρ Oph A ($T = 21$ K and $n_H = 6 \times 10^5$ cm^{-3}) are not typical for dense clouds and lead to an atomic oxygen abundance of $3 \times 10^{-4} n_H$ corresponding to a flux of 7.5×10^5 atoms cm^{-2} s^{-1}. Comparing this to our values of 6.1×10^3 and 1.7×10^4 atoms cm^{-2} s^{-1} it is clear that much more O_2 and HO_2 can be produced. Results of our optimised model run with parameter settings as close as possible to those of ρ Oph A show the following behaviour for the ice abundances $O_3 \gg O_2 > HO_2 > H_2O_2$. If

we assume that the species H_2O_2 and HO_2 are predominantly formed on the grain surface and that the gas phase is a good reflection of the ice composition, our H_2O_2/HO_2 abundance ratio of 0.6 is in good agreement with the observed ratio presented by Parise *et al.*[32] of 1.

As compared to the previous simulations of Cuppen and Herbst[5], our final amount of produced H_2O is similar and varies as a function of A_V. Since the 2007 results were in good agreement with the observations by Whittet *et al.*[41] of water ice in Taurus dark clouds in terms of the water ice threshold value of $A_V = 3.2$ K and linear growth of the column density of water ice above this value. The present results offer a similar agreement. The main differences between the studies are the formation routes for water ice. We expect this to have consequences for the deuterium fractionation of the ice species, although this was unexplored in the present paper. Since some of the channels like $H_2 + OH$ posses a barrier, which can be overcome through quantum chemical tunneling the formation of H_2O will be favoured over HDO. For other channels this might the reverse. Cazaux *et al.*[20] included deuteration reactions in their water ice network to study this effect, unfortunately there is not enough experimental and quantum chemical evidence available to back up this network and to make it predictive.

5 Discussions and conclusions

In the present paper, exothermicity of reactions is used to increase the momentum of the final products by increasing the hopping and desorption rates. Garrod *et al.*[42] showed that chemical desorption can play an important role in explaining the observed abundance of different gas phase chemical species. Later Cazaux *et al.*[20] and Dulieu *et al.*[18] made similar conclusions. Here we see again the same effect. But exothermicity cannot only lead to desorption but can also lead to a more compact ice which has an effect on many diffusion properties and it can allow reactants to meet. In our simulations, we indeed see this compactification.

Here the exothermicity is only considered for reactions with two or more reaction products and the excess energy is only employed for diffusion and desorption and not to overcome chemical reactions. Allowing also single reaction products to desorb with a higher probability, leads to too much desorption under interstellar conditions: even in dense clouds hardly any ice is formed. Applying the excess energy to overcome reactions as well leads to too many $H + H_2O_2$ under experimental conditions. If the energy is not partitioned between the two products according to their relative masses, the desorption rate of OH upon H_2O photodissociation becomes near unity. Our set-up in the current paper therefore best describes experimental and astronomical observations as well as Molecular Dynamics simulations. Moreover, we believe this to be a rather accurate description of the underlying physics and chemistry, where the exothermicity is transferred into kinetic energy. Because of conservation of momentum this can only be done for reaction of multiple products and the energy is distributed considering their relative masses. How excess energy can be applied to overcome chemical barriers is not clear and this mechanism is currently missing in our models. With this Discussions we hope to trigger new dedicated studies and discussions on this topic and on the role of exothermicity in general. Also the role of a kick-out mechanism remains unexplored in this work.

Acknowledgements

References

1   M. J. Drake, *Meteor. Planet. Sci.*, 2005, **40**, 519.

2   K. Muralidharan, P. Deymier, M. Stimpfl, N. H. de Leeuw and M. J. Drake, *Icarus*, 2008, **198**, 400–407.

3   D. Bockelée-Morvan, D. C. Lis, J. E. Wink *et al.*, *Astron. Astrophys.*, 2000, **353**, 1101–1114.

4   E. F. Dishoeck, E. Herbst and D. A. Neufeld, *Chem. Rev.*, 2013, **113**, 9043 and references therein.

5   H. M. Cuppen and E. Herbst, *Astrophys. J.*, 2007, **668**, 294–309.

6   N. Miyauchi, H. Hidaka, T. Chigai, A. Nagaoka, N. Watanabe and A. Kouchi, *Chem. Phys. Lett.*, 2008, **456**, 27–30.

7   E. Matar, E. Congiu, F. Dulieu, A. Momeni and J. L. Lemaire, *Astron. Astrophys.*, 2008, **492**, L17–L20.

8   S. Ioppolo, H. M. Cuppen, C. Romanzin, E. F. van Dishoeck and H. Linnartz, *Astrophys. J.*, 2008, **686**, 1474–1479.

9   Y. Oba, N. Watanabe, T. Hama, K. Kuwahata, H. Hidaka and A. Kouchi, *Astrophys. J.*, 2012, **749**, 67.

10 T. Lamberts, H. M. Cuppen, S. Ioppolo and H. Linnartz, *Phys. Chem. Chem. Phys.*, 2013, **15**, 8287.

11 S. Ioppolo, H. M. Cuppen, C. Romanzin, E. F. van Dishoeck and H. Linnartz, *Phys. Chem. Chem. Phys.*, 2010, **12**, 12065.

12 H. M. Cuppen, L. E. Kristensen and E. Gavardi, *Mon. Not. R. Astron. Soc.*, 2010, **406**, L11–L15.

13 F. Dulieu, IAU Symposium, 2011, pp. 405–415.

14 H. M. Cuppen, L. J. Karssemeijer and T. Lamberts, *Chem. Rev.*, 2013, **113**, 8840.

15 S. Andersson, A. Al-Halabi, G.-J. Kroes and E. F. van Dishoeck, *J. Chem. Phys.*, 2006, **124**, 064715.

16 C. Arasa, S. Andersson, H. M. Cuppen, E. F. van Dishoeck and G. Kroes, *J. Chem. Phys.*, 2010, **132**, 184510.

17 C. Arasa, S. Andersson, H. M. Cuppen, E. F. van Dishoeck and G. J. Kroes, *J. Chem. Phys.*, 2011, **134**, 164503.

18 F. Dulieu, E. Congiu, J. Noble, S. Baouche, H. Chaabouni, A. Moudens, M. Minissale and S. Cazaux, *Sci. Reports*, 2013, **3**, 1338.

19 R. Garrod, I. H. Park, P. Caselli and E. Herbst, *Faraday Discussions*, 2006, **133**, 51.

20 S. Cazaux, V. Cobut, M. Marseille, M. Spaans and P. Caselli, *Astron. Astrophys.*, 2010, **522**, A74.

21 E. F. van Dishoeck, B. Jonkheid and M. C. van Hemert, *Faraday Disc.*, 2006, **133**, 231.

22 R. Atkinson, D. L. Baulch, R. A. Cox, J. N. Crowley, R. F. Hampson, R. G. Hynes, M. E. Jenkin, M. J. Rossi and J. Troe, *Atmos. Chem. Phys.*, 2004, **4**, 1461–1738.

23 D. V. Shalashilin and B. Jackson, *J. Chem. Phys.*, 1998, **109**, 2856–2864.

24 H. M. Cuppen and L. Hornekær, *J. Chem. Phys.*, 2008, **128**, 174707.

25 A. P. J. Jansen, *Comp. Phys. Comm.*, 1995, **86**, 1.

26 E. A. Bergin and M. Tafalla, *Ann. Rev. Astron. Astrophys.*, 2007, **45**, 339–396.

27 Q. Chang, H. M. Cuppen and E. Herbst, *Astron. Astrophys.*, 2005, **434**, 599–611.

28 M. E. Palumbo, *Astron. Astrophys.*, 2006, **453**, 903–909.

29 G. A. Kimmel, Z. Dohnálek, K. P. Stevenson, R. S. Smith and B. D. Kay, *J. Chem. Phys.*, 2001, **114**, 5295–5303.

30 Y. Oba, N. Miyauchi, H. Hidaka, T. Chigai, N. Watanabe and A. Kouchi, *Astrophys. J.*, 2009, **701**, 464–470.

31 P. Bergman, B. Parise, R. Liseau, B. Larsson, H. Olofsson, K. M. Menten and R. Güsten, *Astron. Astrophys.*, 2011, **531**, L8.

32 B. Parise, P. Bergman and F. Du, *Astron. Astrophys.*, 2012, **541**, L11.

33 F. Du and B. Parise, *Astron. Astrophys.*, 2011, **530**, A131.

34 T. I. Hasegawa and E. Herbst, *Mon. Not. R. Astron. Soc.*, 1993, **261**, 83–102.

35 E. Herbst and H. M. Cuppen, *Proc. Natl. Acad. Sci. USA*, 2006, **103**, 12257–12262.

36 A. Yabushita, T. Hama, M. Yokoyama, M. Kawasaki, S. Andersson, R. N. Dixon, M. N. R. Ashfold and N. Watanabe, *Astrophys. J. Lett.*, 2009, **699**, L80–L83.

37 K. I. Öberg, E. F. van Dishoeck and H. Linnartz, *Astron. Astrophys.*, 2009, **496**, 281–293.

38 B. Larsson, R. Liseau, L. Pagani, P. Bergman, P. Bernath, N. Biver, J. H. Black, R. S. Booth, V. Buat, J. Crovisier, C. L. Curry, M. Dahlgren, P. J. Encrenaz, E. Falgarone, P. A. Feldman, M. Fich, H. G. Florén, M. Fredrixon, U. Frisk, G. F. Gahm, M. Gerin, M. Hagström, J. Harju, T. Hasegawa, Å. Hjalmarson, L. E. B. Johansson, K. Justtanont, A. Klotz, E. Kyrölä, S. Kwok, A. Lecacheux, T. Liljeström, E. J. Llewellyn, S. Lundin, G. Mégie, G. F. Mitchell, D. Murtagh, L. H. Nordh, L.-Å. Nyman, M. Olberg, A. O. H. Olofsson, G. Olofsson, H. Olofsson, G. Persson, R. Plume, H. Rickman, I. Ristorcelli, G. Rydbeck, A. A. Sandqvist, F. V. Schéele, G. Serra, S. Torchinsky, N. F. Tothill, K. Volk, T. Wiklind, C. D. Wilson, A. Winnberg and G. Witt, *Astron. Astrophys.*, 2007, **466**, 999–1003.

39 R. Liseau, P. F. Goldsmith, B. Larsson, L. Pagani, P. Bergman, J. Le Bourlot, T. A. Bell, A. O. Benz, E. A. Bergin, P. Bjerkeli, J. H. Black, S. Bruderer, P. Caselli, E. Caux, J.-H. Chen, M. de Luca, P. Encrenaz, E. Falgarone, M. Gerin, J. R. Goicoechea, Å. Hjalmarson, D. J. Hollenbach, K. Justtanont, M. J. Kaufman, F. Le Petit, D. Li, D. C. Lis, G. J. Melnick, Z. Nagy, A. O. H. Olofsson, G. Olofsson, E. Roueff,

A. Sandqvist, R. L. Snell, F. F. S. van der Tak, E. F. van Dishoeck, C. Vastel, S. Viti and U. A. Yıldız, *Astron. Astrophys.*, 2012, **541**, A73.

40 K. I. Öberg, S. Bottinelli and E. F. van Dishoeck, *Astron. Astrophys.*, 2009, **494**, L13–L16.

41 D. C. B. Whittet, P. A. Gerakines, J. H. Hough and S. S. Shenoy, *Astrophys. J.*, 2001, **547**, 872–884.

42 R. T. Garrod, V. Wakelam and E. Herbst, *Astron. Astrophys.*, 2007, **467**, 1103–1115.